AGU PUBLICATIONS

JGR

Journal of Geophysical Research: Space Physics

RESEARCH ARTICLE

10.1002/2013JA019433

Key Points:
- Calculation of fractal dimension of Dst series and solar photosphere
- Evolution of fractal dimensions
- Correlation between solar activity and magnetic storms

Correspondence to:
M. Domínguez,
macadominguez@gmail.com

Citation:
Domínguez, M., V. Muñoz, and J. A. Valdivia (2014), Temporal evolution of fractality in the Earth's magnetosphere and the solar photosphere, *J. Geophys. Res. Space Physics*, *119*, 3585–3603, doi:10.1002/2013JA019433.

Received 10 SEP 2013
Accepted 22 APR 2014
Accepted article online 25 APR 2014
Published online 22 MAY 2014

Temporal evolution of fractality in the Earth's magnetosphere and the solar photosphere

Macarena Domínguez[1], Víctor Muñoz[1], and Juan Alejandro Valdivia[1]

[1]Departamento de Física, Facultad de Ciencias, Universidad de Chile, Santiago, Chile

Abstract The study of complexity in two aspects of the magnetic activity in the Sun-Earth system is presented. We compare the temporal evolution of the magnetic fluctuations in the Earth's magnetosphere and the spatial distribution of the magnetic field in the solar photosphere, by calculating fractal dimensions from the data. It is found that the fractal dimension of the *Dst* data decreases during magnetic storm states and is well correlated with other indexes of solar activity, such as the solar flare and coronal indexes. This correlation holds for individual storms, full-year data, and the complete 23rd solar cycle. The fractal dimension from solar magnetogram data also correlates well with both the *Dst* index and solar flare index, although the correlation is much more clear at the larger temporal scale of the 23rd solar cycle, showing a clear increase around solar maximum.

1. Introduction

Complexity studies in plasma physics have been of great interest as they provide new insights and reveal possible universalities on issues such as geomagnetic activity, turbulence in laboratory plasmas, physics of the solar wind, etc. [*Dendy et al.*, 2007; *Klimas et al.*, 2000; *Takalo et al.*, 1999; *Chang and Wu*, 2008; *Valdivia et al.*, 1988]. In particular, these studies have shown that systems such as the magnetosphere [*Chang*, 1999; *Valdivia et al.*, 2005, 2003, 2006, 2013], the solar wind [*Macek*, 2010], the solar photosphere, and solar corona [*Berger and Asgari-Targhi*, 2009; *Dimitropoulou et al.*, 2009] are in a self-organized critical state and exhibit complex features such as fractality and multifractality.

Most studies have focused on studying some of these features separately. However, due to the coupling between the solar, interplanetary, and Earth's magnetosphere activities, it is interesting to find and understand the possible correlations between the complex features observed in each system. Such study could give us valuable insight into the coupling in the dynamics of these systems and an eventual improvement in the forecast of space weather [*Valdivia et al.*, 2012, 1999a, 1999b].

The fractal dimension of time series, such as records of solar sunspot number or Earth's auroral electrojet index *AE*, or spatial data, such as a solar magnetogram, is one interesting characterization of the complexity of the system, among many other related quantities, that turns out to be in general a noninteger value smaller than the Euclidean dimension [*Aschwanden and Aschwanden*, 2008a, 2008b; *Kozelov*, 2003; *McAteer et al.*, 2005]. Several works have discussed the relationship between fractal and multifractal dimensions with physical quantities, and its relevance to forecast events on the Sun's surface (solar flares), the solar wind, and Earth's magnetosphere [*Aschwanden and Aschwanden*, 2008a; *Uritsky et al.*, 2006; *Georgoulis*, 2012; *McAteer et al.*, 2005, 2010; *Dimitropoulou et al.*, 2009; *Conlon et al.*, 2008; *Chapman et al.*, 2008; *Kiyani et al.*, 2007].

The main objective of this work is to characterize the occurrence of events such as geomagnetic storms and solar flares by means of a fractal dimension, as a way to measure the complexity of magnetic field time series and spatial patterns. In this context, we analyze the possible time correlation between the calculated fractal dimensions and various indexes of geomagnetic and solar dynamics.

In particular, we calculate a box-counting fractal dimension [*Addison*, 1997], because of its simplicity and its intuitive meaning. Although the box-counting algorithm can provide only partial information on the complexity of the systems, in particular when they also exhibit multifractality as in our case, it is able to describe some features of solar and geomagnetic complexity as we will show below, and in fact it has also been successfully used in other studies of the Sun-Earth system [*Osella et al.*, 1997; *Kozelov*, 2003; *Gallagher et al.*, 1998; *Georgoulis*, 2012; *Lawrence et al.*, 1993; *Cadavid et al.*, 1994; *McAteer et al.*, 2005].

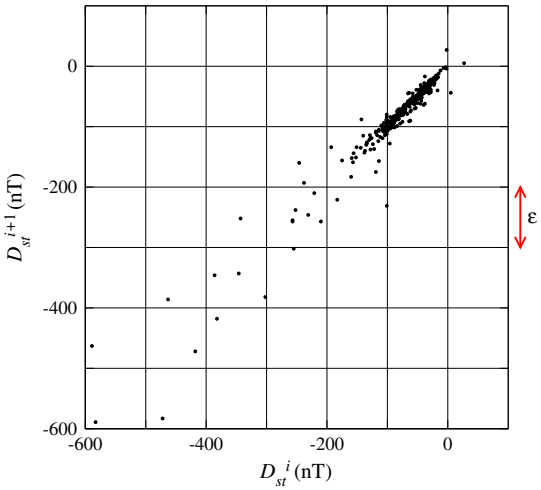

Figure 1. Scatter diagram for the hourly *Dst* time series corresponding to the first storm state (6 to 20 March) 1989. (More details in section 3.) The size of the square box is ϵ.

Thus, the box-counting dimension gives us a fast approach to systematically study the complexity properties of solar and geomagnetic activity and a first step to detect possible correlations between them.

The analysis was made with hourly data for the *Dst* index (World Data Center for Geomagnetism, Kyoto, http://wdc.kugi.kyoto-u.ac.jp/caplot/index.html) and daily magnetograms of the solar photosphere (Solar Oscillations Investigations (SOI) project, http://soi.stanford.edu/magnetic/index5.html). It should be noted that calculation of the fractal dimension for the *Dst* series is based on a scatter diagram [see, e.g., *Witte and Witte*, 2009], whereas previous studies have been done with other methods or data [*Kozelov*, 2003; *Uritsky et al.*, 2006; *Balasis et al.*, 2006; *Dias and Papa*, 2010]. On the other hand, previous magnetogram studies have typically focused on relating the fractal dimension of the local magnetic field configuration in a zone of the Sun's surface to the flare emission in the same zone. Here we perform this analysis with the whole surface to have a global quantification of the complexity of the Sun.

To this end, we study events during 5 years of high geomagnetic activity, namely, 1960, 1989, 2000, 2001, and 2003. We also analyze the complete 23rd solar cycle, in order to understand to what extent the conclusions drawn for particular events are robust and can be extrapolated to years with arbitrary levels of solar activity.

The paper is organized as follows. In section 2 we present the method to calculate the fractal dimension for the *Dst* time series. Then, in the following three sections, sections 3–5, we present the results obtained with the *Dst* time series. Geomagnetic storms are first located, and then three different types of windows around storms are used to analyze the data. Then, solar magnetograms are studied in section 6. The method to calculate the fractal dimension for a magnetogram is presented, and results are compared with those for the *Dst* time series. In section 7 we perform the same analysis for the *Dst* index and solar magnetograms but for the full 23rd solar cycle. Finally, in section 8 results are summarized and discussed.

2. *Dst* Time Series: Fractal Dimension

Complexity in the Earth's magnetosphere is studied by estimating the fractal dimension of the hourly *Dst* time series (World Data Center for Geomagnetism, Kyoto, http://wdc.kugi.kyoto-u.ac.jp/caplot/index.html).

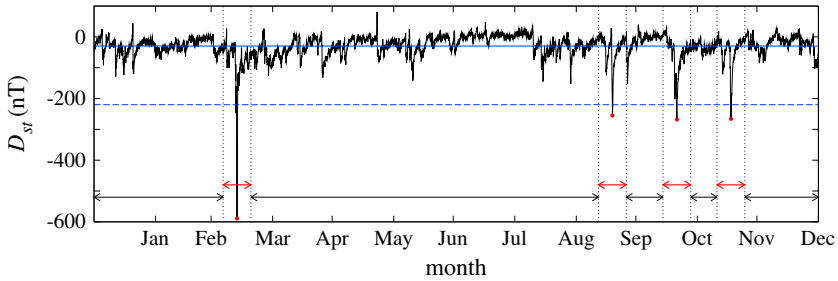

Figure 2. *Dst* time series for 1989, identifying the storm and quiet states as explained in section 3. The solid horizontal line shows the average value, and the dashed horizontal line the threshold value used to identify a geomagnetic storm. Red dots show the minimum *Dst* value identified in Table 1. Red and black arrows show windows corresponding to storm and quiet states, respectively.

Table 1. Minimum Value of the Peaks Where *Dst* < −220 nT[a]

Date	State	Minimum *Dst* Value (nT)
1 Apr 1960	2	−327
30 Apr 1960	4	−325
6 Oct 1960	6	−287
13 Nov 1960	8	−339
13 Mar 1989	2	−589
18 Sep 1989	4	−255
19 Oct 1989	6	−268
17 Nov 1989	8	−266
6 Apr 2000	2	−288
15 Jul 2000	4	−301
12 Aug 2000	6	−235
30 Mar 2001	2	−387
11 Apr 2001	3	−271
6 Nov 2001	5	−292
30 Oct 2003	2	−383
20 Nov 2003	4	−422

[a]Each minimum value occurs, by definition, at the center of a storm state. States are labeled by consecutive integers within a year (see Figure 3, where the same labeling is used). In this manner, the first and second storms in the year are labeled 2 and 4, respectively, because there are quiet states in between.

There are several ways to construct a fractal dimension of a time series, leading to several alternative definitions for the dimension. For instance, in the time domain, one can calculate the Hurst exponent of the series, which can be related to the box-counting dimension of the graph of the time series or the scaling of the power spectra. Also, plotting the time series and regarding it as a curve on a plane, one can cover the curve with equal-size boxes, equal-size segments, or equal-radius spheres and then either count the number of units needed to cover the plot or count the number of points within each unit, thus leading to the box-counting, divider, correlation dimension, etc. [*Addison*, 1997; *Theiler*, 1990]. In general, there is no simple way to relate these quantities, other than the fact that they can be nonintegers and thus they are measures of the complexity of the set. In our case, the fractal dimension is estimated by the box-counting method [*Addison*, 1997] in the way we now describe. First, we construct a scatter diagram for each *Dst* time series. If Dst^i is the ith *Dst* datum in the series and N is the total number of data, the scatter diagram is a plot of Dst^{i+1} versus Dst^i, for $1 \leq i \leq N-1$, as shown in Figure 1.

Then, the scatter diagram is divided into square cells of a certain size ϵ, and we count the number $N(\epsilon)$ of cells which contain a point. Next, we consider several values of ϵ, and we find the range of ϵ where $\log(N(\epsilon))$ scales linearly with $\log \epsilon$. If the slope in the linear regime is given by $-D$, then in this region,

$$N(\epsilon) \propto \epsilon^{-D}, \tag{1}$$

where D represents the scatter diagram box-counting dimension. The least squares fit for the slope also provides an estimation of the error in D. Since *Dst* data have no associated error, all points have the same weight in the linear fit.

Even though there are other measures of the complexity of a time series, this measure is simple and quick enough to use, even with long data sets. Furthermore, the scatter plot itself provides an interesting way to visualize the complexity of a time series, as fully random behavior would yield a uniform filling of the bidimensional space whereas nontrivial self-correlations would result in other patterns, features which have been proposed, for instance, as methods to diagnose heart diseases [*Acharya et al.*, 2014; *Hoshi et al.*, 2013].

Now in order to calculate the fractal dimension, a certain time frame of the *Dst* series must be chosen. In the following sections the box-counting dimension is calculated for three types of time windows.

In principle, since the *Dst* time series is not stationary in general (although it can be regarded as such during quiet periods), one should expect results to be sensitive to the time windows width. However, our main results are qualitatively independent of it, as we will show in the next sections.

3. *Dst* Time Series: Storm and Quiet States

We first apply this technique to quiet and active periods with magnetic storms in order to investigate the relationship between the intensity of the *Dst* index and its fractal dimension, a relationship which has also been suggested by other studies of the complexity of the *Dst* series [*Balasis et al.*, 2009; *Papa and Sosman*, 2008].

First, we need to define "storm states" and "quiet states," so that we start by locating the peaks in the *Dst* series where $Dst < -220$ nT. A geomagnetic storm has three phases [*Tsurutani and Gonzalez*, 1994;

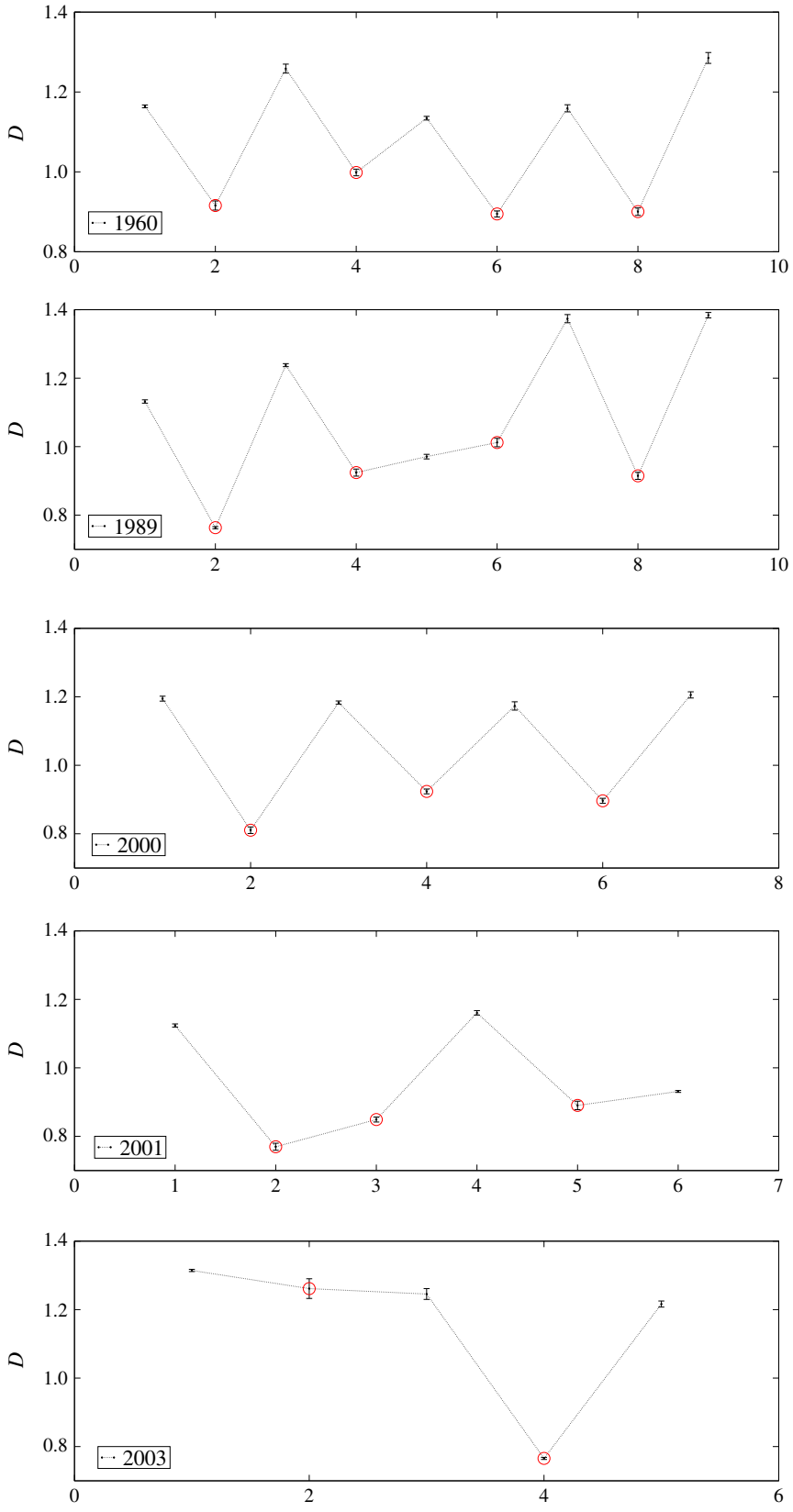

Figure 3. Box-counting dimension *D* for storm and quiet states for the years studied. The abscissa represents the labeling of the states as explained in section 3. Red circles indicate storm states.

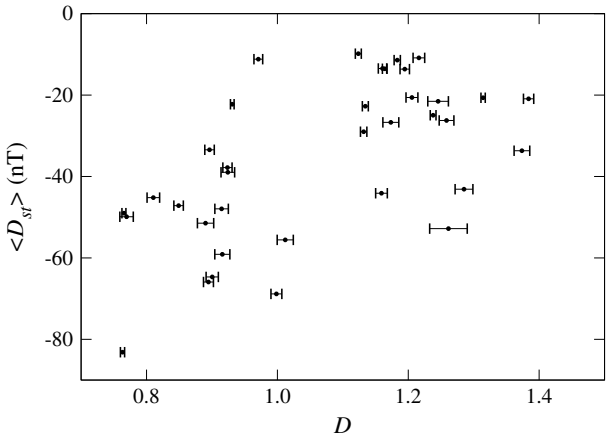

Figure 4. Mean value of *Dst* for each state as a function of the box-counting dimension *D* with respective error bars (calculated as in Figure 3). All years in Figure 3 are included.

Gonzalez et al., 1994]: an initial phase (which takes minutes to hours to complete, and *Dst* can reach tens of nanoteslas), the main phase (takes between 30 min and several hours, and *Dst* can reach hundreds of nanoteslas), and a recovery phase (from tens of hours to a week, where the magnetic variation level returns back to normal). Based on this, we define a "storm state" as a window starting 1 week before the minimum value of the peak and ending 1 week after it. The "quiet state" corresponds to the period of time between two "storm states." To illustrate this, Figure 2 shows the four peaks detected in 1989 and the corresponding windows.

For future identification, we label each state in a year with consecutive integer numbers, starting from 1. For instance, in Figure 2, the year starts with a quiet state, then that will be state "1"; the following state will be a storm, and it will be state "2." Thus, all future quiet states within the year will be labeled with consecutive odd numbers, whereas storm states will be labeled with consecutive even numbers.

Table 1 shows all the peaks found in the years studied, their minimum *Dst* value, and the corresponding label according to the definition above.

Performing the procedure described in section 2, we calculate the box-counting dimension for each storm and quiet state for the 5 years of study. Results are shown in Figure 3, using the labels defined above to identify states. Red circles indicate storm states. Error bars in *D* are given by the error of the least squares linear fit as mentioned in section 2.

We note that in general, a storm state has a smaller fractal dimension than the surrounding quiet states. However, it is not possible to determine a global criterion as to how small *D* is during a storm state. In effect, as shown in Figure 4, a plot of the mean value of *Dst* for each state as a function of the box-counting dimension does not reveal a clear relationship between them when several storms and years are taken into account. In Figure 4 all states for all years in Figure 3 are included. No obvious correlation is found if individual years are considered either.

4. *Dst* Time Series: Variable Width Windows Around a Storm

As a second way to study how fractal dimension is correlated with the existence of a geomagnetic storm, we calculate the fractal dimension for windows of variable size around a storm. If the qualitative connection between fractal dimension and existence of a storm observed in section 3 is robust, then widening the window around a storm should increase its fractal dimension, as more "quiet" data are taken into account.

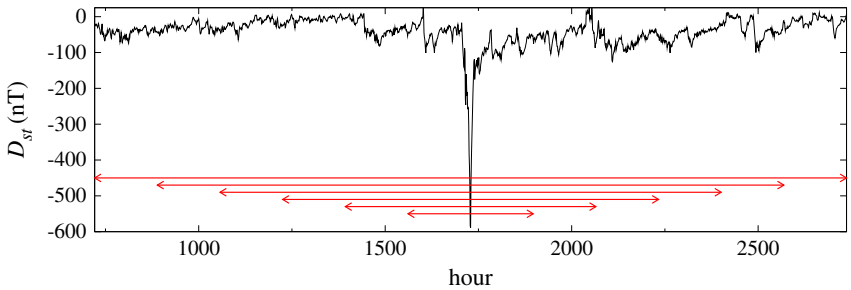

Figure 5. Variable size windows around the 13 March 1989 storm (peak at abscissa 1729). The plot shows the *Dst* index as a function of time, measured in hours since the beginning of the year.

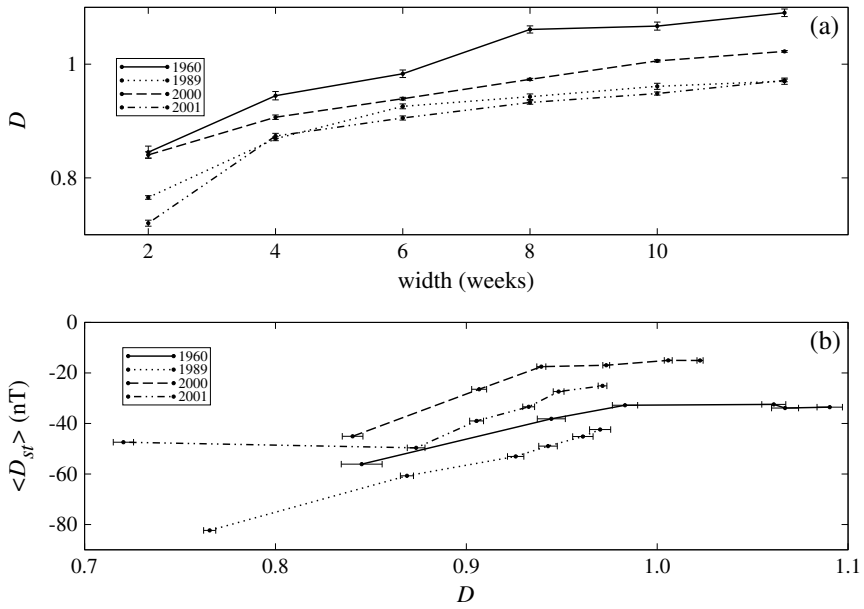

Figure 6. (a) Box-counting dimension *D* for a storm state with respective error bars, as a function of the width of the window around it. (b) Mean value of *Dst* for each variable width window around the same storms in Figure a, as a function of the box-counting dimension with respective error bars.

To this end, we take windows starting/ending *n* weeks before/after the peak, with $n = 1, \ldots, 6$. We illustrate this in Figure 5, where the windows considered around the 13 March 1989 storm are shown.

Figure 6a shows the results for four particular storms: 1 April 1960, 13 March 1989, 6 April 2000, and 30 March 2001, with minimum intensities of −327 nT, −589 nT, −288 nT, and −387 nT, respectively. These storms have been chosen because they are isolated, so that windows can be enlarged (up to 4 weeks on each side) without including new "storm states." In the case of 2001, the two storm states detected are too close (separated by about 2 weeks, which is within the minimum window width we considered), so we regard these events as a single one.

We note that the box-counting dimension increases when we zoom out from the storm, a result which is consistent with those in section 3, because as we widen the window around the storm, the relevance of the storm itself decreases, and the window should become more similar to a quiet state, thus increasing the value of its fractal dimension.

In order to detect a possible correlation between the fractal dimension and the *Dst* value, we plot the mean value of *Dst* in a window as a function of *D* (see Figure 6b), for the same storms as in Figure 6a. It is interesting to note that all curves exhibit a region of almost linear dependence between *D* and *Dst*. This is consistent with Figures 6a and 3. Increasing the window width leads to an increase in *D*, as more and more "quiet state" data are included. Similarly, it is expected that as we increase the window width we should also increase the

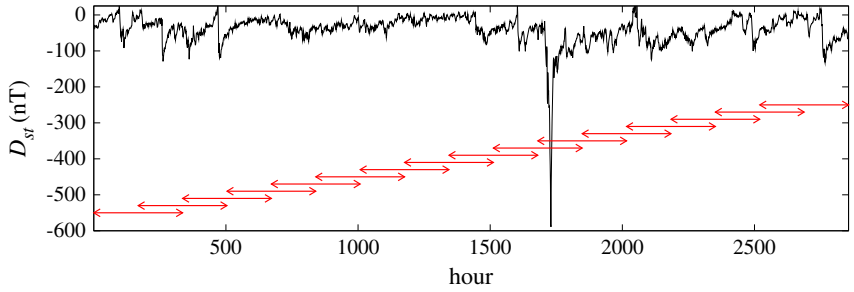

Figure 7. Moving windows across a storm (13 March 1989).

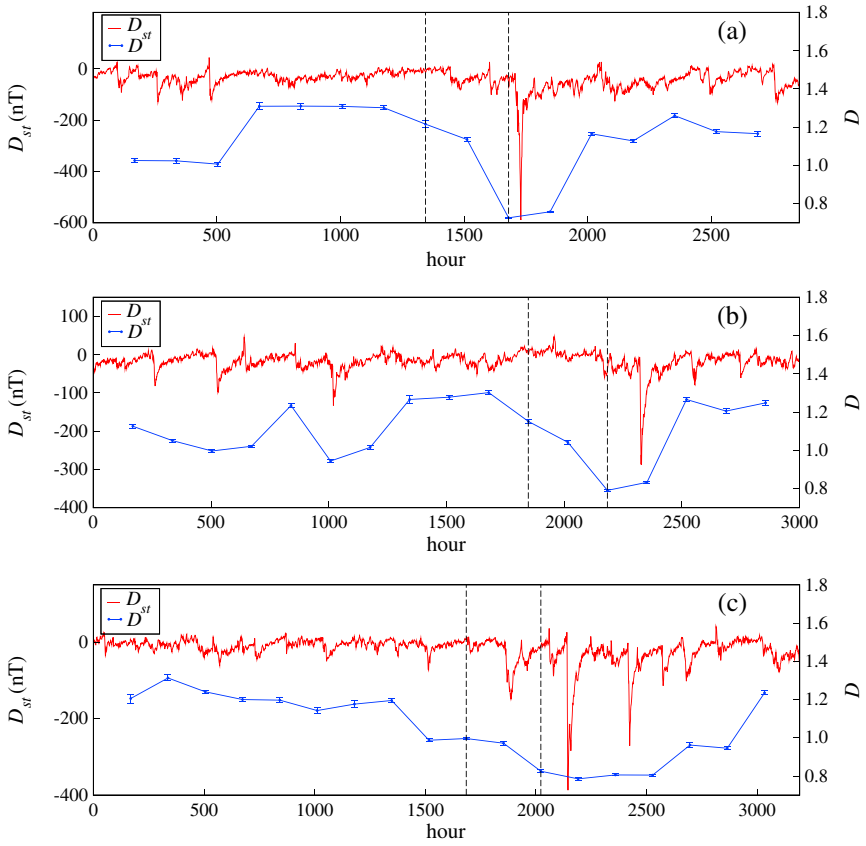

Figure 8. Box-counting dimension D (blue, with error bars) and *Dst* index (red) for storms: (a) 13 March 1989, (b) 6 April 2000, and (c) 30 March 2001, with moving windows. Vertical lines show windows of data where D decreases before the storm.

average value of *Dst* for the same reason. Hence, a linear relation between the two quantities should not be too surprising as the method increasingly selects the fractal dimension of the fractal with the largest weight.

However, Figure 6b also shows that this linear behavior is broken, and this is due to the existence of nearby peaks near the observed storm and the distance between both peaks. Let us consider, for instance, the 1989 event. It is a very isolated storm, as seen in Figure 10b (the first large peak, near hour 2000). The previous argument is valid for all window widths, and D and $\langle Dst \rangle$ vary linearly. In the year 2001 (see first major peak near the hour 2000 in Figure 10d), the situation is different. It is enough to double the width of the window from 2 to 4 weeks to include the nearby peak. Thus, $\langle Dst \rangle$ should not increase, as the window is still dominated by a storm regime. Further increasing the window width captures more "quiet state" data. Consistent with this, the first two points in the 2001 curve in Figure 6b lie almost in a horizontal line, and the next points show a linear behavior with positive slope. In year 1960 there is also a close second peak but at a larger distance (see Figure 10a), so it is necessary to have wider windows to include both; this is why the break in the linear behavior is observed on the right part of the curve in Figure 6b.

The smaller range of widths in which the linear dependence is observed in years 1960, 2000, and 2001, compared with 1989, is also consistent with the fact that the peak value of *Dst* for these three storms is smaller, so they reach the average value $\langle Dst \rangle$ of the surrounding quiet states for a smaller window.

We can also note in Figure 6b that, in the range where they are linear, there seems to be one slope common for 2000 and 2001 and another one common for 1960 and 1989. This may be related to variations in the properties of the solar wind, such as average speed or active time, and consistent with the idea that the level of burstiness depends on the activity level (or strength of solar wind driver) as suggested by *Wanliss and Uritsky* [2010]. However, since the effect is not consistent over all storms, a more quantitative explanation may not be possible with our characterization of complexity using fractal dimensions.

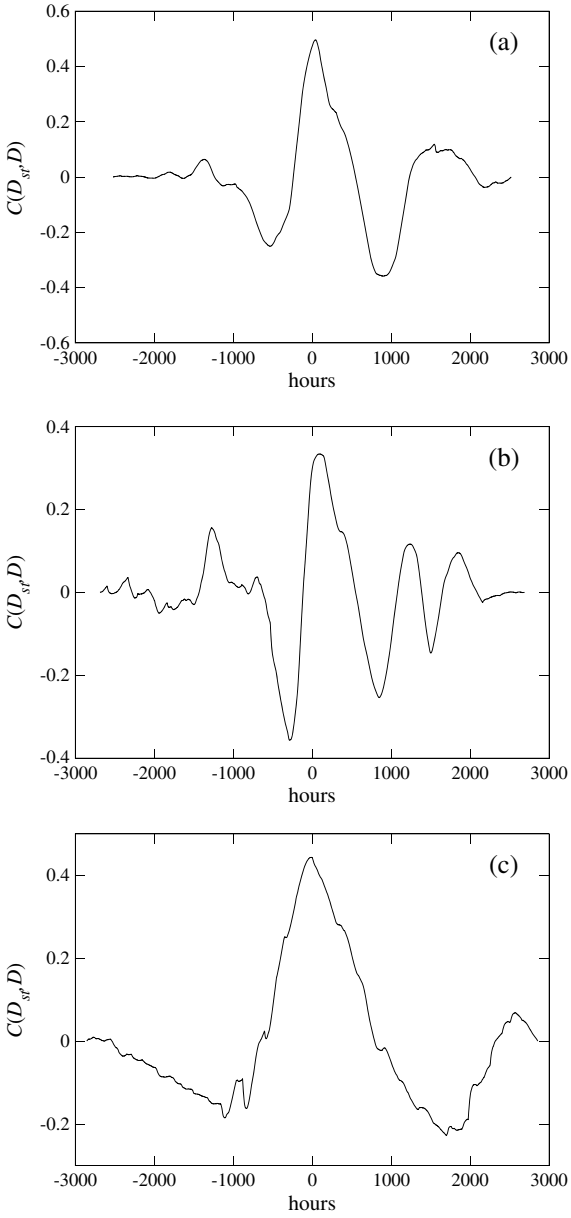

Figure 9. Normalized cross correlation between *Dst* and *D*. (a) 13 March 1989 storm; (b) 6 April 2000 storm; and (c) 30 March 2001 storm (see Figure 8).

5. *Dst* Time Series: Moving Windows Across a Storm

The results in sections 3 and 4 show that the fractal dimension decreases during a geomagnetic storm. In order to investigate the evolution of the fractal dimension of the *Dst* index, as a representation of the complexity of the ring current dynamics, we now calculate the fractal dimension for fixed width windows (2 weeks), initially placed well before the storm peak, and move it in steps of 1 week crossing the peak.

We take the same storms for the years 1989, 2000, and 2001. In all cases, we place the window initially in the first day of the year and move it until it reaches the third week after the peak (see Figure 7).

As in the previous section, we calculate the box-counting dimension for each window of data using the same method described in section 2. Figure 8 shows the results obtained and compares them with *Dst* index.

In all cases studied, the box-counting dimension of the *Dst* index decreases as the storm approaches. However, it is very interesting to note that we have a noticeable change in the fractal dimension, even before the window contains any point of the geomagnetic storm, as defined by its three phases. This is illustrated in Figure 8, where two vertical lines have been drawn to indicate the window of *Dst* immediately before the storm. The storm is not included in the window; however, the fractal dimension has already started to decrease.

Of course, the minimum value of the box-counting dimension of the *Dst* index occurs at the windows containing the *Dst* peak. In order to appreciate this effect in a more systematic way, we calculate a cross correlation between *Dst* and *D*. To do so, we first interpolate the data for *D* in order to have the same 1 h resolution as the *Dst* time series. We use a simple linear interpolation, which will be enough to estimate the correlation in this case. Calculation of the cross correlation between *Dst* and *D* yields a distinctive positive peak at zero lag, at least for the 1989 and 2001 storms, whereas a peak is also observed for the 2000 storm, although not clearly dominant (see Figure 9).

In order to study whether the effect found in Figure 8 is global rather than valid for the few particular storms we checked, we repeated the analysis but for the same five complete years studied throughout this paper (1960, 1989, 2000, 2001, and 2003), which have already been analyzed but only near geomagnetic storms.

Figure 10 shows that, as concluded before, the box-counting dimension consistently decreases when the storm approaches, thus suggesting that the box-counting dimension of the *Dst* series, or similar measures of complexity, could be of relevance when forecasting geomagnetic storms.

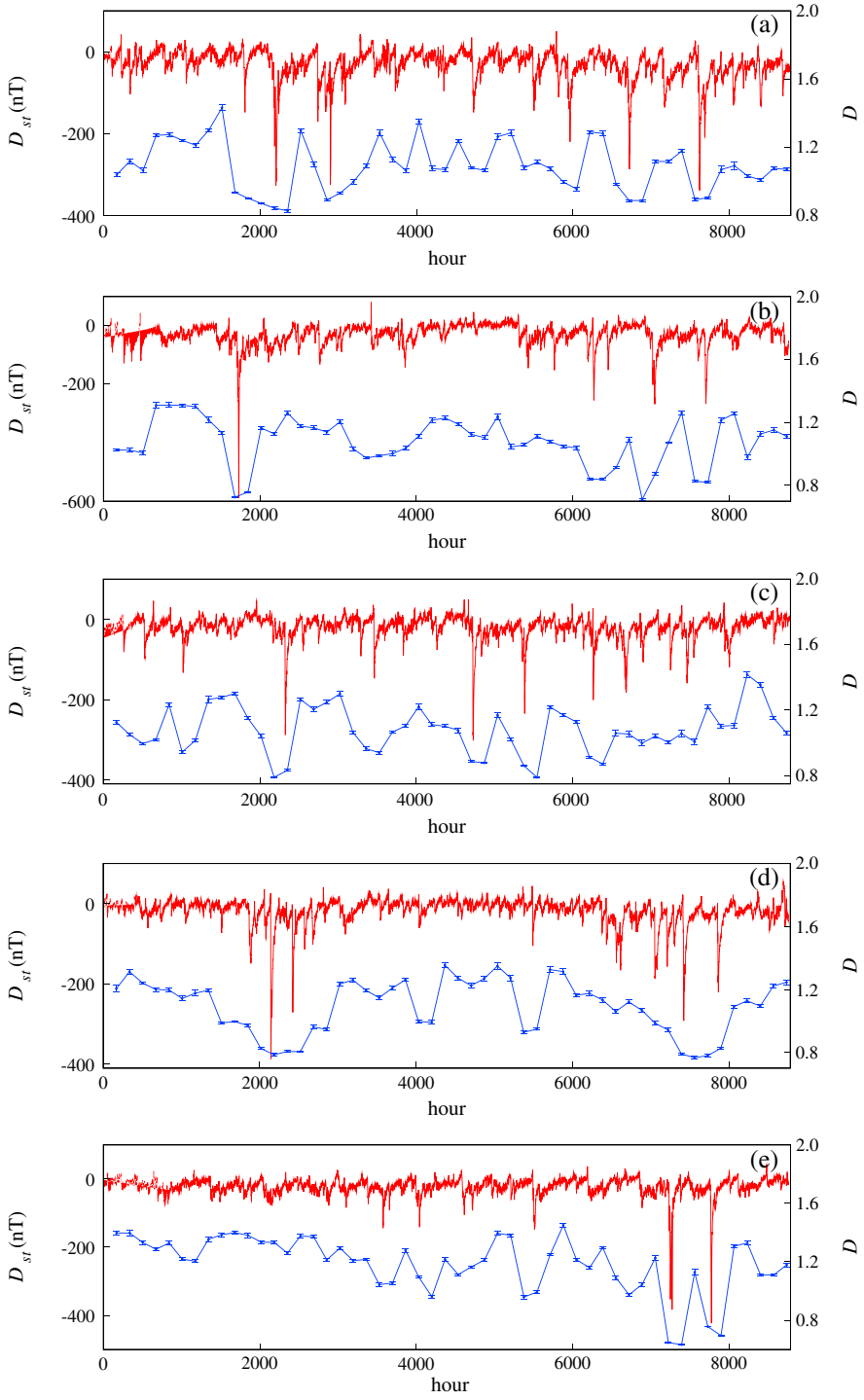

Figure 10. Box-counting dimension for 5 years in the active solar phase. Red lines correspond to the *Dst* time series. Blue lines correspond to the box-counting dimension *D* for each moving window. Error bars for *D* points have been included. (a) 1960; (b) 1989; (c) 2000; (d) 2001; and (e) 2003.

This can also be observed in the cross correlation of *Dst* and *D*, where a distinctive peak near zero lag can be observed for all years. As an illustration, Figure 11 shows three of them.

Geomagnetic activity is certainly linked to solar activity as both local events, such as coronal mass ejections, and global features, such as the solar cycle, have impact on the Earth's magnetosphere, as seen for instance in auroral dynamics. It is thus interesting to study whether there is a signature of this in the evolution of

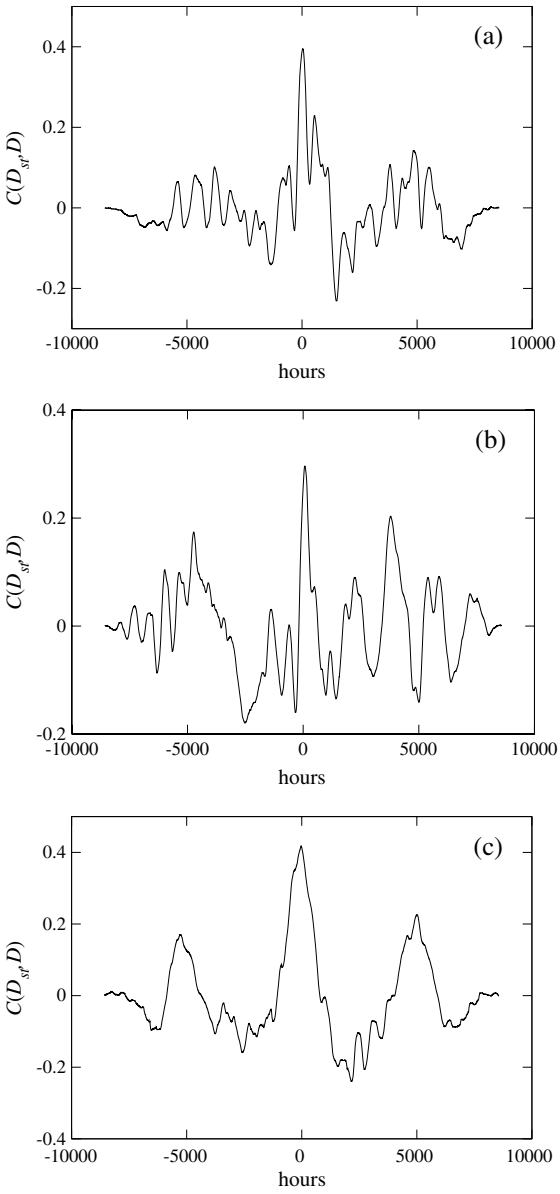

Figure 11. Normalized cross correlation between *D* and *Dst* for full-year data. (a) 1960; (b) 1989; and (c) 2001.

fractal dimensions as calculated here. We will now analyze the possible correlation between the complexity in the *Dst* and some indexes characterizing the solar activity, by comparing the fractal dimension associated with the *Dst* time series to the solar flare index and the coronal index (National Geophysical Data Center (NOAA), Solar Data Services, http://www.ngdc.noaa.gov/stp/solar), which are measures of energy released from the Sun as explained below.

Solar flare index corresponds to daily flare activity over a 24 h period. It is roughly proportional to the total energy emitted by the flare and is a measure of the short-lived activity on the Sun [*Ataç and Özgüç*, 1998; *Özgüç et al.*, 2003]. In this manuscript, we consider the total solar flare index (sum of Northern and Southern Hemispheres indexes), averaged over the same windows we use to calculate the fractal dimension *D* in Figure 10.

Results are shown in Figure 12 (left). Notice that all three subfigures have the same vertical and horizontal scales. This permits us to show that even for solar flare events of different intensities, periods of large solar flare index are accompanied by a decrease in the fractal dimension *D* of the *Dst* time series. This is very clear for the 1989 event, Figure 12a, and somewhat less obvious but still clear for 2001, Figure 12b. For the 2000 event it is not evident, though.

Another quantity proposed to characterize solar magnetic activity is the coronal index (National Geophysical Data Center (NOAA), Solar Data Services, http://www.ngdc.noaa.gov/stp/solar). It represents the average daily power (irradiance) emitted by the green corona into 1 sr toward the Earth [*Rybanský et al.*, 2001]. As we did with the solar flare index analysis above, we average the coronal index over the same windows used to calculate the fractal dimension *D* and plot results in Figure 12 (right).

We note that, approximately 1 or 2 weeks before the minimum value of *D*, which corresponds to the storm, there is a maximum in the coronal index. However, this is only clearly seen regarding positions of maximum/minimum values. A more detailed correlations analysis using daily coronal index data does not show any particular signature.

We observe that two different estimations of solar activity are correlated to some extent with *D*, thus suggesting a link between the solar activity and the fractal features of the Earth's magnetosphere. Certainly, one should probably not expect to find a single index to reveal this, as geomagnetic dynamics may be mostly but not exclusively determined by solar behavior and several other correlated pairs have been proposed [*Yurchyshyn et al.*, 2004], but it is interesting to notice the overall consistency of the results, at least when a correlation can be observed. In this sense, it is also worth mentioning the fact that even though the

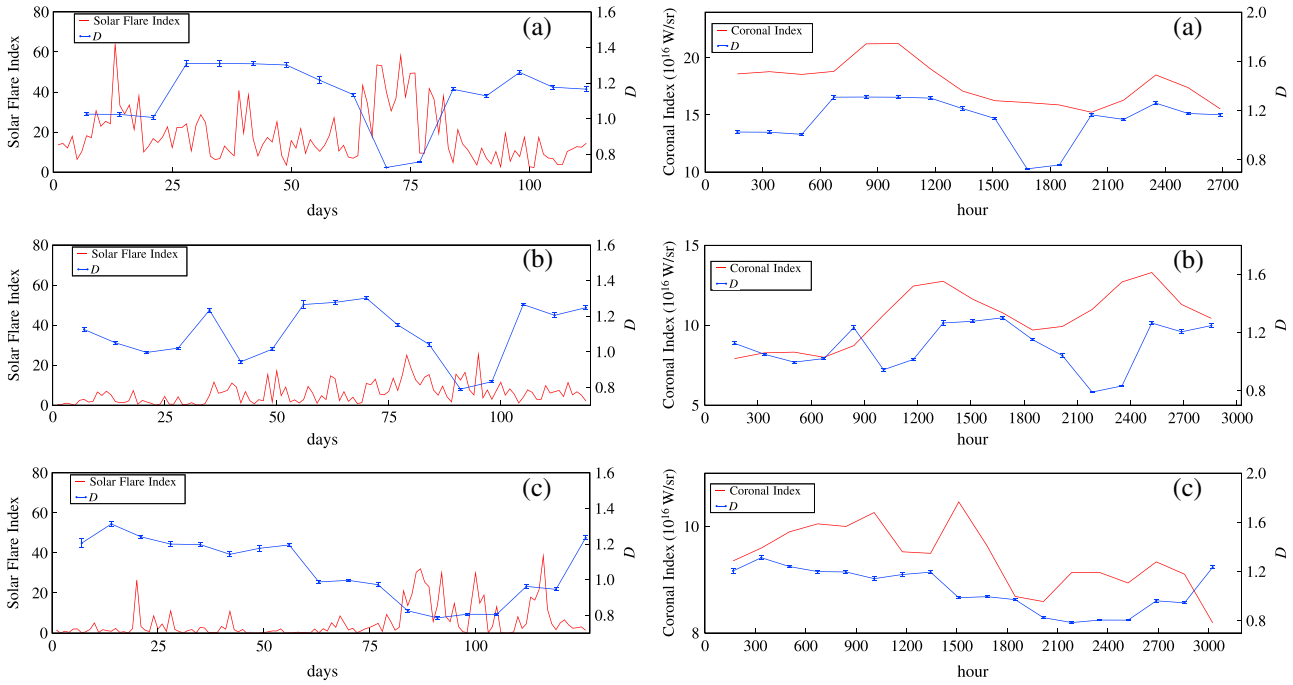

Figure 12. Box-counting dimension *D* (with error bars) corresponding to the *Dst* index, along with the (left) solar flare and (right) coronal indexes for the storms: (a) 13 March 1989, (b) 6 April 2000, and (c) 30 March 2001, with moving windows.

connection between the solar flare index and *D* is not clear for the 2000 event (Figure 12b, left), the apparent 2 weeks lag between the coronal index and *D* is observed for the same event (Figure 12b, right).

6. Magnetograms: Fractal Dimension

The evolution of the *Dst* time series studied in the previous sections is largely influenced by solar activity. In order to further investigate a possible relationship between fractal features in geomagnetic and solar dynamics, we now study the fractal properties of the magnetic field configuration on the solar surface.

To this aim, we analyze daily magnetograms taken from Michelson Doppler Imager (MDI) Daily Magnetic Field Synoptic Data (Solar Oscillations Investigations (SOI) project, http://soi.stanford.edu/magnetic/index5.html) [*Yang and Zhang*, 2012]. These are averages of several observations collected over the course of a 27 day solar rotation, thus representing the magnetic field strength on the solar disk.

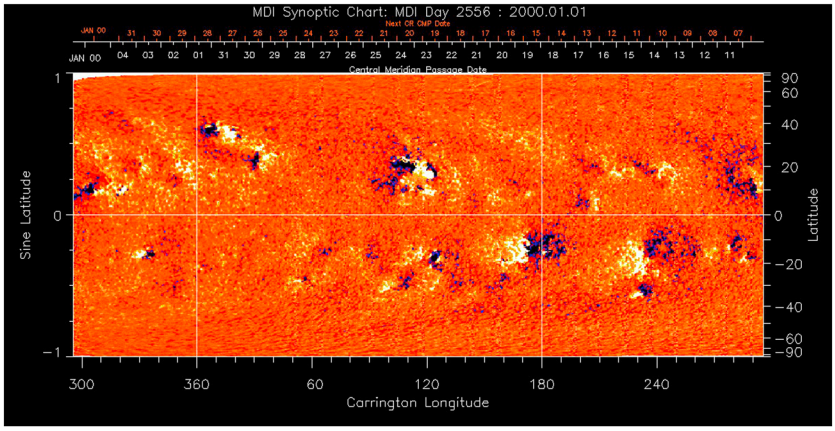

Figure 13. Magnetogram for 1 January 2000.

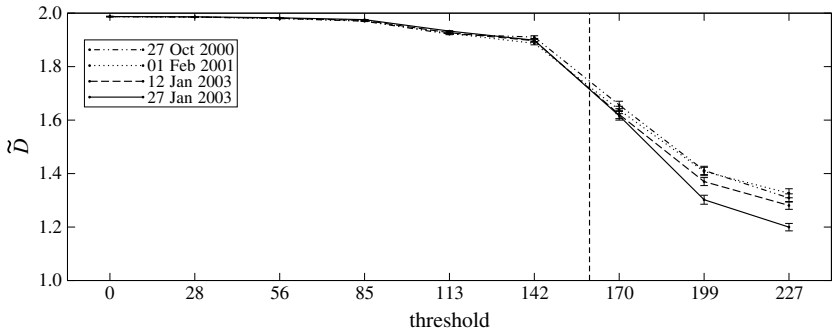

Figure 14. Box-counting dimension $\tilde{D}$ for the four chosen magnetograms, using 10 different values for the threshold α (see text). The vertical line marks the chosen threshold, $\alpha = 155$.

We take three complete years: 2000, 2001, and 2003. Notice that in sections 3–5 we have studied 1960, 1989, 2000, 2001, and 2003. We intend to compare the analysis in the current section with the full-year analysis in section 5. However, there is no magnetogram data for 1960 and 1989, so we ignore them in this section. A typical magnetogram image is shown in Figure 13.

Various studies have proposed the calculation of fractal dimensions, either by using the box-counting algorithm or others, to study the complex dynamics of the solar surface. For instance, the fractal dimension in active regions has been calculated by using a perimeter/area relation [*Meunier*, 1999; *Paniveni et al.*, 2010], the box-counting algorithm [*McAteer et al.*, 2005], or the correlation integral method [*Uritsky and Davila*, 2012]. Lists of calculated fractal dimensions using various methods can be found in *McAteer et al.* [2005] and *Aschwanden and Aschwanden* [2008a], while comparisons with numerical simulations are discussed by *Janssen et al.* [2003]. These methods have also been applied to analyze images in other scenarios such as the complex topology of magnetic fields that leads to energy release events, or for auroral dynamics [*Kozelov*, 2003].

The multifractal nature of the dynamics on the solar surface has been studied, particularly in active regions [*Lawrence et al.*, 1993; *Cadavid et al.*, 1994; *Uritsky and Davila*, 2012; *Uritsky et al.*, 2013]. The ability of fractal and multifractal analysis to be forecasting tools for flare appearance, or to correlate with indexes of solar activity like the solar flare index or sunspot number, has been discussed by *Georgoulis* [2012], *Vertyagina and Kozlovskiy* [2013], *Abramenko* [2005], and *Abramenko and Yurchyshyn* [2010].

In order to properly calculate a box-counting dimension for a MDI Daily Magnetic Field Synoptic Data, we need to consider projection effects. Several studies where a fractal dimension is calculated for MDI full disk magnetograms [*McAteer et al.*, 2005; *Georgoulis*, 2012] have dealt with the problem of distortion by analyzing only data within 60° of the solar disk center. In our case, we consider full magnetogram images such as Figure 13, but for all images, activity is concentrated within 60° of the solar equator anyway, so the contribution of points beyond this latitude is indeed marginal and does not affect our conclusions.

In order to calculate a box-counting dimension from Figure 13, the first step is to make the scatter diagram, which involves converting the image into a pattern of 0 and 1 values, or equivalently black and white points, where 1 (white) pixels are associated with large magnetic field intensity (as defined below). The scatter diagram itself will be given by the set of white points, over which we can calculate the box-counting dimension with the same method presented in section 2.

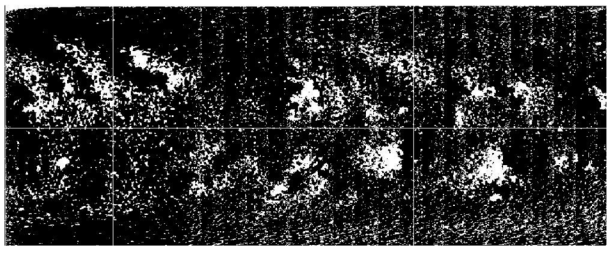

Figure 15. Black-and-white pattern obtained from the magnetogram in Figure 13, using a threshold $\alpha = 155$.

Obtaining a black-and-white pattern from a color magnetogram like Figure 13 is a two-step process: first we transform the image to gray scale using MATLAB. (The algorithm eliminates the hue and saturation and retains the luminance; see, e.g., MATLAB rgb2gray function, http://www.mathworks.com/help/images/ref/rgb2gray.html.) Now that

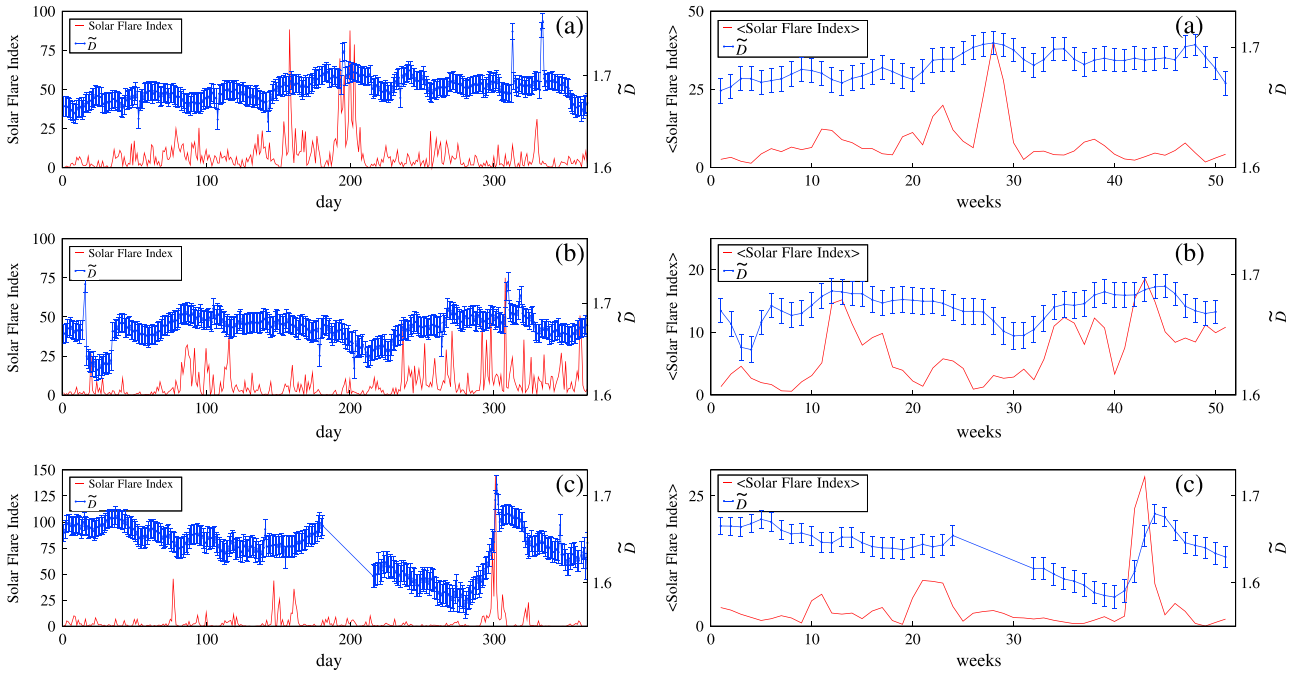

Figure 16. (left) Fractal dimension of magnetograms and solar flare index and (right) averaged over moving windows in (a) 2000, (b) 2001, and (c) 2003. The error in the regression of $\tilde{D}$ is included as error bars. The gap in the blue curve in Figure 16c is due to the lack of magnetogram data for this period in 2003.

the image is only a pattern of intensities, coded in the image files as integer numbers from 0 (black) to 255 (white), we choose a certain threshold intensity α, above (below) which a point is considered white (black). Finally, the box-counting dimension $\tilde{D}$ of the high-intensity (white) region is calculated.

The nontrivial part of this procedure is the choice of a proper threshold. If α is too small, then the resulting image would be essentially white; if α is too high, the image would be essentially black. So, an appropriate value of α must be found, such that the complex features of the pattern are retained. In order to make a decision, we choose four magnetograms randomly and calculate the box-counting dimension for all the images that result by choosing several possible values of α between 0 and 255. Results are shown in Figure 14.

Observing Figure 14, we choose $\alpha = 155$ noting that around this value the box-counting dimension $\tilde{D}$ is not so sensitive to the choice of α while still retaining fractal features of the pattern (noninteger values of $\tilde{D}$).

Notice that the dependence of the fractal dimension on the threshold is an indication of the multifractal nature of the system, as each threshold makes visible structures on different scales [*Abramenko*, 2005].

Figure 15 shows the black-and-white pattern which results from processing Figure 13 using $\alpha = 155$. Based on patterns like this, for each daily magnetogram available, the box-counting dimension is calculated.

Results for all magnetograms in the years 2000, 2001, and 2003 are presented in Figure 16 (left), where they are plotted along with the solar flare index for the same window, as a way to compare the fractal dimension with the occurrence of solar flares.

First, we notice that the box-counting dimension is clearly a noninteger value, which is consistent with previous results focused specifically on active regions [*Lawrence et al.*, 1993; *Cadavid et al.*, 1994; *Paniveni et al.*, 2010; *Uritsky and Davila*, 2012; *Uritsky et al.*, 2013; *Janssen et al.*, 2003].

We also observe some relationship between box-counting dimension and solar flare index: the box-counting dimension tends to increase when the solar flare index is higher. However, it is a weak effect, and the calculation of the cross correlation does not show any clear trend.

This effect can be somewhat better noted when averaging both the magnetogram fractal dimension and the solar flare index over moving time windows. We take windows of width equal to 2 weeks, as in the *Dst* analysis in section 5. Results are shown in Figure 16 (right) for the years 2000, 2001, and 2003.

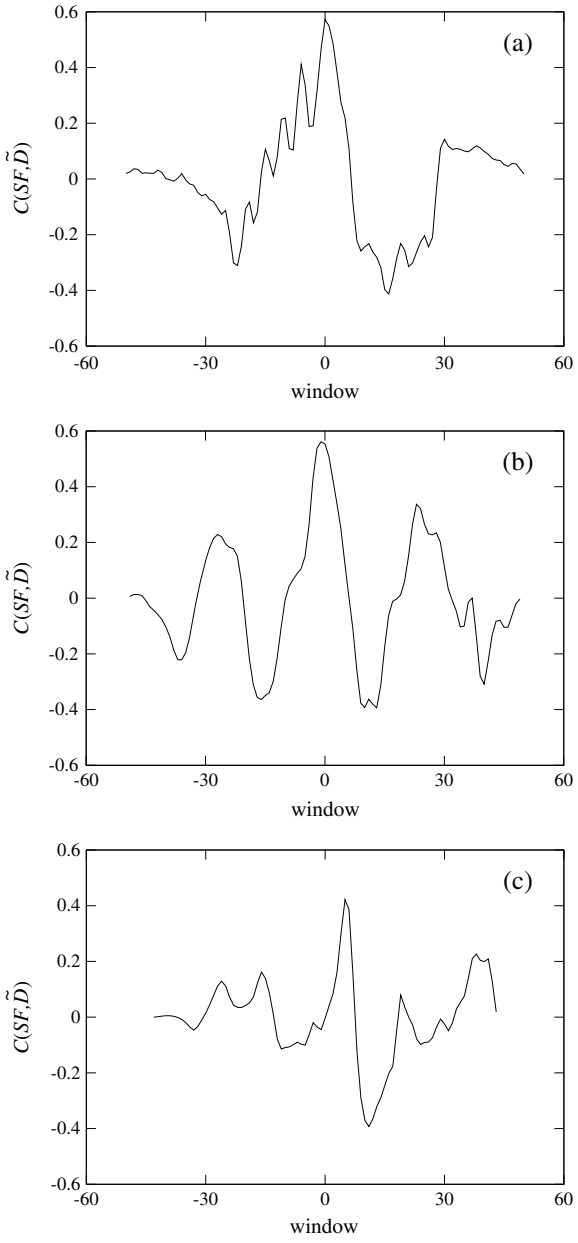

Figure 17. Normalized cross correlation between solar flare index and $\tilde{D}$ for full-year data, averaged over moving windows 2 weeks wide. (a) 2000; (b) 2001; and (c) 2003.

We can note, at least in Figure 16b, that the relationship between $\tilde{D}$ and the solar flare index is slightly more evident in the averaged analysis. A cross-correlation calculation between $\tilde{D}$ and solar flare index confirms this observation, except for the 2003 case, where solar flare data seem to lag behind $\tilde{D}$ (see Figure 17).

In order to check whether the magnetogram fractal dimension can be related to magnetic activity in the Earth's magnetosphere, we compare it with the *Dst* time series, for the same years as in section 6. This is shown in Figures 18a–18c.

No evident consistent correlation is observed between both quantities. In fact, the cross correlation between them does not exhibit any clear trend.

7. Analysis for 23rd Solar Cycle

Until now, we have performed all the analyses for a few years, selected because of their high magnetospheric activity, the presence of isolated storms, and the availability of *Dst* and/or magnetogram data for them. In order to investigate whether the conclusions drawn for those particular years also hold for years of various degrees of solar and magnetospheric activity, in this section we study the evolution of the fractal dimension of the *Dst* time series and of the magnetogram data for a complete solar cycle (the 23rd).

As in section 3, we first find all geomagnetic storms, then we define storm and quiet states as we did in section 3, and then we calculate the box-counting dimension within those states. Results are presented in Figure 19 (left) and are consistent with those in section 3: a storm state has a smaller fractal dimension than the surrounding quiet states.

We also perform a study with moving windows, similar to that in section 5, except that windows are 3 months wide, and they are moved in steps of 1.5 months (width of the windows was chosen in order to have smooth curves). Thus, since we have a larger data set, we can see whether the features observed at short time scales, spanning a single storm event, are also observed at larger time scales. Figure 19 (right) shows the results obtained for the *Dst* time series.

Again, results are consistent with those in section 5: the *Dst* box-counting dimension decreases when a geomagnetic storm approaches. And in fact, the cross correlation between *Dst* and *D* also for 23rd solar cycle exhibits a peak near zero lag.

Finally, we calculate the box-counting dimension $\tilde{D}$ for magnetograms in the 23rd cycle, using the same method and threshold value α as described in section 6. The resulting fractal dimension is shown as a blue

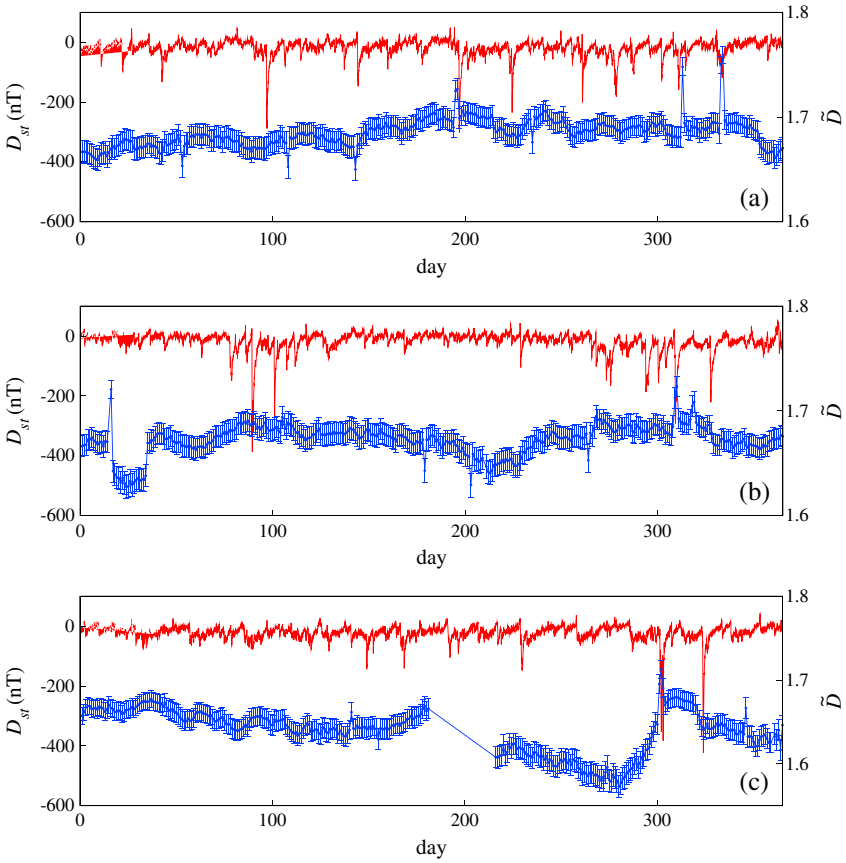

Figure 18. Fractal dimension of magnetograms (blue line, with error bars) and *Dst* index (red line) in (a) 2000, (b) 2001, and (c) 2003.

line in Figure 20. (We have found that the jump at the end of the solar cycle and the narrow peak at its center are due to problems with the original magnetogram data, where vertical stripes, such as those seen on the right of Figure 15, are increasingly prominent in the images. In spite of this, the general trend is very clear.)

Figure 20a shows the comparison between $\tilde{D}$ and *Dst*, suggesting that larger values of the fractal dimension correspond to periods of larger magnetospheric activity. We notice that we could not draw this conclusion

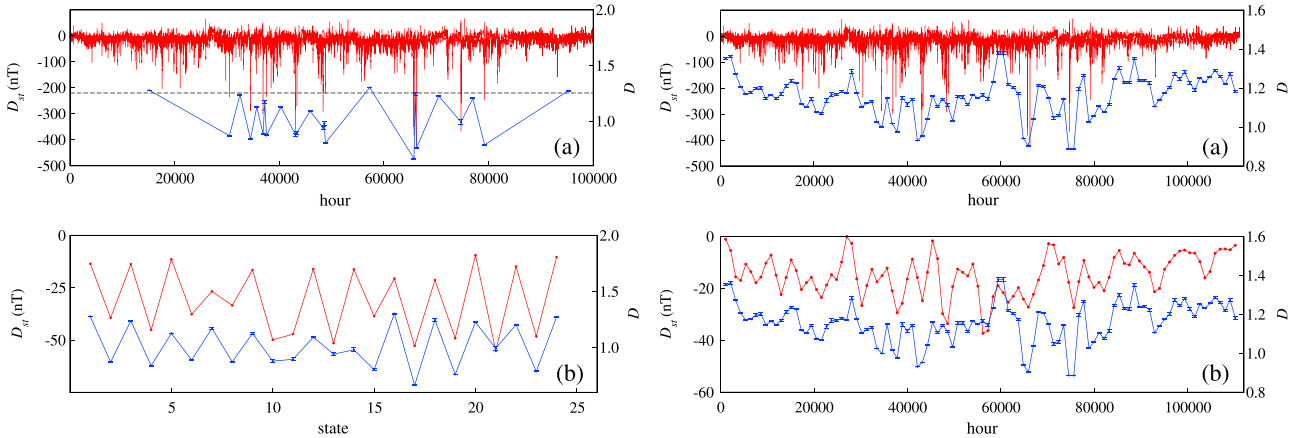

Figure 19. *Dst* time series analysis: (left) Box-counting dimension *D* for storm and quiet states and (right) moving windows for the 23rd cycle (blue line, with error bars) and respective *Dst* index (red line). (a) Using hourly data for *Dst* and (b) using average *Dst* over the respective window.

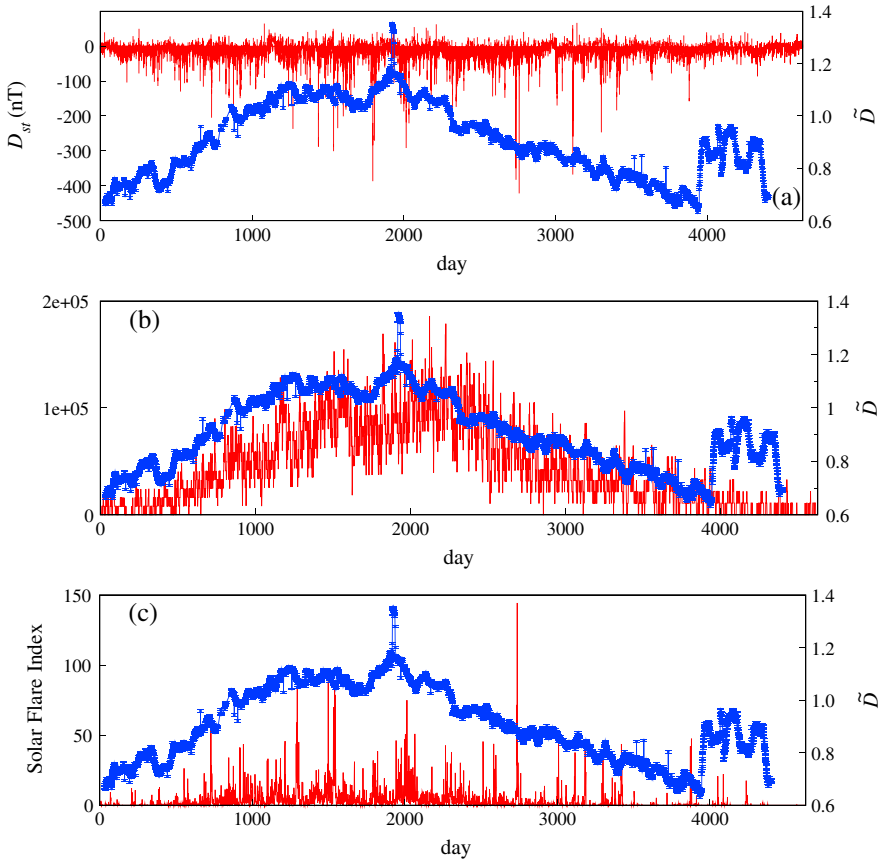

Figure 20. Magnetograms analysis. Blue line: Daily box-counting dimension $\tilde{D}$ for the 23rd cycle, with error bars. Red line: (a) *Dst* index; (b) sunspot number; and (c) solar flare index.

from the full-year analysis in section 6. This suggests that, at least for large time scales, it is possible to find a relationship between the fractal features of the solar photosphere and geomagnetic activity on Earth.

It is also interesting to investigate its possible correlation with solar activity. To this end, in Figure 20b, the fractal dimension $\tilde{D}$ is compared with sunspot number. Larger values of the fractal dimension correspond to periods of larger solar activity as measured by the sunspot number, a connection which is much more clear than in Figure 20a. A similar result can also be observed, although less conclusively, when comparing $\tilde{D}$ with the solar flare index (Figure 20c).

8. Discussion and Summary

In this paper, we have studied the evolution of the complexity present in the magnetic dynamics of the Earth's magnetosphere and the solar photosphere, by using *Dst* time series and daily magnetograms, respectively. In both cases, we calculated the fractal dimension with the box-counting method and using data corresponding to 5 years of high activity in the *Dst* index: 1960, 1989, 2000, 2001, and 2003. In addition, comparison of these fractal dimensions with various indexes of solar activity (in particular, solar flare index, coronal index, and sunspot number) was performed.

It is found that in general the fractal dimension D of the *Dst* time series decreases during a geomagnetic storm, a decrease which we observed by averaging over three different types of time windows and which starts a few days before *Dst* reaches its minimum value. Although no clear correlation between the values of D and *Dst* is observed, the decrease of the fractal dimensions during a magnetic storm is a very robust finding in the data sets analyzed, as confirmed by cross-correlation analyses, which typically yield a maximum at zero lag.

In order to investigate a possible correlation between the fractal dimension of the *Dst* series and solar activity, a comparison between D and both the solar flare and coronal indexes was made. It was found that, even

for solar flares of different intensities, periods of large solar flare index are accompanied by a decrease in the fractal dimension *D*, at least for two of the three storm events analyzed. As to the coronal index, noticeable descents of the fractal dimension *D* are observed to occur about 2 weeks after a peak in the solar coronal index.

The fact that two different estimations of solar activity are correlated to some extent with the fractal dimension of the *Dst* suggests that the relation between solar and Earth's magnetosphere dynamics can also be observed when looking at the fractal features of the magnetic fluctuations measured at the Earth.

All the analyses above were performed for single, isolated storm events, and the significance of these findings could be limited to the particular events examined. Taking this into account, we repeated the comparison between *D* and *Dst* for the five complete years studied throughout this paper. Inspection of both time series yields the same result as above, that is, the box-counting dimension for the *Dst* data consistently decreases when the storm approaches. Besides the fact that the cross correlation between *D* and *Dst* yields a clear positive peak at zero lag, a clear decrease in *D* may be observable before the start of the storm (as defined above), thus suggesting that the fractal dimension could be of relevance for the forecasting of geomagnetic storms.

Regarding the photospheric dynamics, as measured by the magnetograms, comparisons between its fractal dimension $\tilde{D}$ and both a magnetospheric index (*Dst*) and a solar index (solar flare) were performed. A weak connection between $\tilde{D}$ and the solar flare index is observed, a correlation which is slightly more evident when the time series are smoothed over 2 week windows, as shown by cross-correlation calculations. No particular signature was observed when comparing the magnetogram fractal dimension with the *Dst* index, either by inspection of the respective time series or by cross-correlation calculations.

In order to check whether our choice of five separated years has biased our results, we also compared *Dst* data, fractal dimension for *Dst*, fractal dimension for magnetograms, and solar flare index, for the complete 23rd solar cycle. On this large-scale analysis we have also found that the fractal dimension *D* decreases during geomagnetic storms and the cross correlation between *D* and *Dst* shows a positive peak near zero lag, as in the case of individual storms and full-year data, showing that the results are qualitatively independent of the length of the sample. This is interesting, as it means that although the *Dst* time series is nonstationary in general, robust qualitative conclusions can be obtained by calculating the box-counting dimension.

Regarding magnetogram data, it is interesting to notice that the weak or essentially null correlation between its fractal dimension and both the *Dst* index and the solar flare index, as obtained from full-year analysis, is much more evident when the large scale of the 23rd solar cycle is considered. In effect, the fractal dimension of the solar magnetogram shows an evident increase around solar maximum and clearly correlates with the corresponding decrease in *Dst* index and the increase in sunspot number, which suggests that $\tilde{D}$ could also be useful to characterize the evolution of activity along a solar cycle. It is worth noticing, though, that solar flare index is not so clearly correlated with the magnetogram fractal dimension.

Given the rich and complex dynamics governing solar magnetic evolution, Earth's magnetic fluctuations, and the interaction between them, it would be very unlikely that a single index would be able to capture all the relevant information. Thus, we have compared several time series. In that sense, it is interesting that some robust conclusions can actually be drawn from the fractal analysis performed: first, the fractal dimension of the *Dst* index consistently decreases around periods of large magnetic perturbation, as measured by the *Dst* index, and of large solar activity, as measured by the solar flare and coronal indexes. These findings hold both for individual, isolated storms and for larger-scale, full-year data and the complete 23rd solar cycle. Some hints that this fractal dimension could be useful as a precursor for large geomagnetic storms, and that the coronal index can be a precursor for the decrease in the fractal dimension, are found, although such hints are not always clear for all data sets and more studies are needed in order to establish the robustness of this observation.

On the other hand, although the fractal dimension of the solar magnetogram data shows a weak correlation with *Dst* and solar flare index for full-year data, at the larger scale of the complete 23rd solar cycle a clear correlation is also observed.

It is expected that the correlations found, specially associated to the complexity variations, may give some insight on the underlying mechanisms governing the interaction between the Sun and the Earth's magnetic field. For instance, previous studies have found that the degree of multifractality in solar wind fluctuations

correlate with the solar cycle, suggesting the existence of regimes dominated by the coronal driver and others by local turbulence [*Chapman et al.*, 2008]. Also, the existence (and absence) of correlation of the scaling of geomagnetic indexes with the energy input from the solar wind into the magnetosphere again suggests that some indexes are more sensitive to the solar driver than others [*Hnat et al.*, 2005]. In our case, the decrease in fractal dimension associated to the *Dst* time series during storm states may be a signature of transitions to a driver-dominated regime. Similarly, the correlations we observed with the solar flare and coronal index could be associated to the impact of variations in the complexity of the solar activity on the Earth's magnetosphere. However, correlations do not manifest themselves in the same way for both indexes, showing that the coupling is by no means simple and that the magnetosphere responds in different ways to various features of the driver. Finally, in the case of magnetograms, it is expected that variations in solar activity are related to the fractal dimension of the magnetic field configurations, as changes in magnetic field topology lead to reconnection events which in turn result in energy release. Our results are consistent with previous, local studies, which focus on small regions on the solar surface [*Paniveni et al.*, 2010; *McAteer et al.*, 2005; *Uritsky and Davila*, 2012; *Uritsky et al.*, 2013]. However, as noted in *Georgoulis* [2012], fractal features of the solar surface may not be proper tools for flare appearance forecast. For the particular case of $\tilde{D}$ we notice that its variation is negligible at time scales of 1 year, so no useful information can be drawn. However, when larger time scales, like the complete solar cycle, are considered, variations in $\tilde{D}$ are evident, and correlated with other indexes of solar activity, so it seems that slower dynamical processes are relevant for solar surface complexity as measured by its fractal dimension.

There are many ways in which the analysis presented here can be improved, either by calculating other fractal dimensions, applying multifractal methods, or considering projection and averaging effects on the magnetograms in order to obtain more precise conclusions.

However, our results suggest that the fractal dimension is an interesting proxy for complexity in the Sun-Earth system, not only for static data but also when the evolution of solar and geomagnetic activities are followed. This is consistent with previous findings obtained by using other measures of complexity, other indexes of magnetic activity, and local rather than global spatial data on the solar surface.

Acknowledgments

This project has been financially supported by FONDECYT under contracts 1110135 (J.A.V.), 1110729 (J.A.V.), 1130273 (J.A.V.), 1080658 (V.M.), and 1121144 (V.M.). M.D. also thanks CONICYT for a doctoral fellowship. We are also thankful for financial support by CEDENNA (J.A.V).

Philippa Browning thanks the reviewers for their assistance in evaluating this paper.

References

Abramenko, V., and V. Yurchyshyn (2010), Intermittency and multifractality spectra of the magnetic field in solar active regions, *Astrophys. J.*, *722*(1), 122–130.

Abramenko, V. I. (2005), Multifractal analysis of solar magnetograms, *Sol. Phys.*, *228*, 29–42.

Acharya, U. R., O. Faust, V. Sree, G. Swapna, R. J. Martis, N. A. Kadri, and J. S. Suri (2014), Linear and nonlinear analysis of normal and CAD-affected heart rate signals, *Comput. Methods Programs Biomed.*, *113*, 55–68.

Addison, P. S. (1997), *Fractals and Chaos, An Illustrated Course*, vol. 1, 2nd ed., Institute of Physics Publishing, Bristol and Philadelphia.

Aschwanden, M. J., and P. D. Aschwanden (2008a), Solar flare geometries. I. The area fractal dimension, *Astrophys. J.*, *674*(1), 530–543.

Aschwanden, M. J., and P. D. Aschwanden (2008b), Solar flare geometries. II. The volume fractal dimension, *Astrophys. J.*, *674*(1), 544–553.

Ataç, T., and A. Özgüç (1998), Flare index of solar cycle 22, *Sol. Phys.*, *180*(1–2), 397–407.

Balasis, G., I. A. Daglis, P. Kapiris, M. Mandea, D. Vassiliadis, and K. Eftaxias (2006), From pre-storm activity to magnetic storms: A transition described in terms of fractal dynamics, *Ann. Geophys.*, *24*(12), 3557–3567.

Balasis, G., I. A. Daglis, C. Papadimitriou, M. Kalimeri, A. Anastasiadis, and K. Eftaxias (2009), Investigating dynamical complexity in the magnetosphere using various entropy measures, *J. Geophys. Res.*, *114*(9), A00D06, doi:10.1029/2008JA014035.

Berger, M. A., and M. Asgari-Targhi (2009), Self-organized braiding and the structure of coronal loops, *Astrophys. J.*, *705*(1), 347–355.

Cadavid, A. C., J. K. Lawrence, A. A. Ruzmaikin, and A. Kayleng-Knight (1994), Multifractal models of small-scale solar magnetic fields, *Astrophys. J.*, *429*, 391–399.

Chang, T. (1999), Self-organized criticality, multi-fractal spectra, sporadic localized reconnection and intermittent turbulence in the magnetotail, *Phys. Plasmas*, *6*, 4137–4145.

Chang, T., and C. C. Wu (2008), Rank-ordered multifractal spectrum for intermittent fluctuations, *Phys. Rev. E*, *77*(4), 045,401.

Chapman, S. C., B. Hnat, and K. Kiyani (2008), Solar cycle dependence of scaling in solar wind fluctuations, *Nonlinear Processes Geophys.*, *15*(3), 445–455.

Conlon, P. A., P. T. Gallagher, R. T. J. McAteer, J. Ireland, C. A. Young, P. Kestener, R. J. Hewett, and K. Maguire (2008), Multifractal properties of evolving active regions, *Sol. Phys.*, *248*(2), 297–309.

Dendy, R. O., S. C. Chapman, and M. Paczuski (2007), Fusion, space and solar plasmas as complex systems, *Plasma Phys. Controlled Fusion*, *49*, A95–A108, doi:10.1088/0741-3335/49/5A/S08.

Dias, V. H. A., and A. R. R. Papa (2010), Statistical properties of global geomagnetic indexes as a potential forecasting tool for strong perturbations, *J. Atmos. Sol. Terr. Phys.*, *72*(1), 109–114.

Dimitropoulou, M., M. Georgoulis, H. Isliker, L. Vlahos, A. Anastasiadis, D. Strintzi, and X. Moussas (2009), The correlation of fractal structures in the photospheric and the coronal magnetic field, *Astron. Astrophys.*, *505*(3), 1245–1253.

Gallagher, P. T., K. J. H. Phillips, L. K. Harra-Murnion, and F. P. Keenan (1998), Properties of the quiet Sun EUV network, *Astron. Astrophys.*, *335*(2), 733–745.

Georgoulis, M. K. (2012), Are solar active regions with major flares more fractal, multifractal, or turbulent than others?, *Sol. Phys.*, *276*(1), 161–181.

Gonzalez, W. D., J. A. Joselyn, Y. Kamide, H. W. Kroehl, G. Rostoker, B. T. Tsurutani, and V. M. Vasyliunas (1994), What is a geomagnetic storm?, *J. Geophys. Res.*, *93*(A4), 5771–5792.
Hnat, B., S. C. Chapman, and G. Rowlands (2005), *J. Geophys. Res.*, *110*, A08206, Scaling and a Fokker-Planck model for fluctuations in geomagnetic indices and comparison with solar wind as seen by Wind and ACE, doi:10.1029/2004JA010824.
Hoshi, R. A., C. M. Pastre, L. C. Marques Vanderlei, and M. Fernandes Godoy (2013), Poincaré plot indexes of heart rate variability: Relationships with other nonlinear variables, *Auton. Neurosci.*, *177*, 271–274.
Janssen, K., A. Vögler, and F. Kneer (2003), On the fractal dimension of small-scale magnetic structures in the Sun, *Astron. Astrophys.*, *409*, 1127–1134.
Kiyani, K., S. C. Chapman, B. Hnat, and R. M. Nicol (2007), Self-similar signature of the active solar corona within the inertial range of solar-wind turbulence, *Phys. Rev. Lett.*, *98*, 211101, doi:10.1103/PhysRevLett.98.211101.
Klimas, A. J., J. A. Valdivia, D. Vassiliadis, D. N. Baker, M. Hesse, and J. Takalo (2000), Self-organized criticality in the substorm phenomenon and its relation to localized reconnection in the magnetospheric plasma sheet, *J. Geophys. Res.*, *105*(A8), 18,765–18,780.
Kozelov, B. V. (2003), Fractal approach to description of the auroral structure, *Ann. Geophys.*, *21*(9), 2011–2023.
Lawrence, J. K., A. A. Ruzmaikin, and A. C. Cadavid (1993), Multifractal measure of the solar magnetic field, *Astrophys. J.*, *417*, 805–811.
Macek, W. M. (2010), Chaos and multifractals in the solar wind, *Adv. Space Res.*, *46*(4), 526–531.
McAteer, R. J., P. T. Gallagher, and P. A. Conlon (2010), Turbulence, complexity, and solar flares, *Adv. Space Res.*, *45*(9), 1067–1074.
McAteer, R. T. J., P. T. Gallagher, and J. Ireland (2005), Statistics of active region complexity: A large-scale fractal dimension survey, *Astrophys. J.*, *631*(1), 628–635.
Meunier, N. (1999), Fractal analysis of Michelson Doppler Imager magnetograms: A contribution to the study of the formation of solar active regions, *Astrophys. J.*, *515*(2), 801–811.
Osella, A., A. Favetto, and V. Silbergleit (1997), A fractal temporal analysis of moderate and intense magnetic storms, *J. Atmos. Sol. Terr. Phys.*, *59*(4), 445–451.
Özgüç, A., T. Ataç, and J. Rybák (2003), Temporal variability of the flare index (1966–2001), *Sol. Phys.*, *214*(2), 375–396.
Paniveni, U., V. Krishan, J. Singh, and R. Srikanth (2010), Activity dependence of solar supergranular fractal dimension, *Mon. Not. R. Astron. Soc.*, *402*(1), 424–428, doi:10.1111/j.1365-2966.2009.15889.x.
Papa, A. R. R., and L. P. Sosman (2008), Statistical properties of geomagnetic measurements as a potential forecast tool for strong perturbations, *J. Atmos. Sol. Terr. Phys.*, *70*(7), 1102–1109.
Rybanský, M., V. Rušin, and M. Minarovjech (2001), Coronal index of solar activity, *Space Sci. Rev.*, *95*(1–2), 227–234.
Takalo, J., J. Timonen, A. Klimas, J. Valdivia, and D. Vassiliadis (1999), Nonlinear energy dissipation in a cellular automaton magnetotail field model, *Geophys. Res. Lett.*, *26*(13), 1813–1816.
Theiler, J. (1990), Estimating fractal dimension, *J. Opt. Soc. Am. A*, *7*(6), 1055–1073.
Tsurutani, B. T., and W. D. Gonzalez (1994), The causes of geomagnetic storms during solar maximum, *EOS Trans. AGU*, *75*(5), 49–53.
Uritsky, V. M., and J. M. Davila (2012), Multiscale dynamics of solar magnetic structures, *Astrophys. J.*, *748*(1), 60, doi:10.1088/0004-637X/748/1/60.
Uritsky, V. M., A. J. Klimas, and D. Vassiliadis (2006), Analysis and prediction of high-latitude geomagnetic disturbances based on a self-organized criticality framework, *Adv. Space Res.*, *37*(3), 539–546.
Uritsky, V. M., J. M. Davila, L. Ofman, and A. J. Coyner (2013), Stochastic coupling of solar photosphere and corona, *Astrophys. J.*, *769*(1), 62, doi:10.1088/0004-637X/769/1/62.
Valdivia, J. A., G. M. Milikh, and K. Papadopoulos (1988), Model of red sprites due to intracloud fractal lightning discharges, *Radio Sci.*, *33*, 1655–1666.
Valdivia, J. A., D. Vassiliadis, A. Klimas, and A. S. Sharma (1999a), Modeling the spatial structure of the high latitude magnetic perturbations and the related current systems, *Phys. Plasmas*, *6*(11), 4185–4194, doi:10.1063/1.873684.
Valdivia, J. A., D. Vassiliadis, A. Klimas, A. S. Sharma, and K. Papadopoulos (1999b), Spatiotemporal activity of magnetic storms, *J. Geophys. Res.*, *104*(A6), 12,239–12,250.
Valdivia, J. A., A. Klimas, D. Vassiliadis, V. Uritsky, and J. Takalo (2003), Self-organization in a current sheet model, *Space Sci. Rev.*, *107*(1–2), 515–522.
Valdivia, J. A., J. Rogan, V. Muñoz, L. Gomberoff, A. Klimas, D. Vassiliadis, V. Uritsky, S. Sharma, B. Toledo, and L. Wastavino (2005), The magnetosphere as a complex system, *Adv. Spa. Res.*, *35*, 961–971.
Valdivia, J. A., J. Rogan, V. Muñoz, and B. Toledo (2006), Hysteresis provides self-organization in a plasma model, *Space Sci. Rev.*, *122*, 313–320.
Valdivia, J. A., A. S. Sharma, and K. Papadopoulos (2012), Prediction of magnetic storms by nonlinear models, *Geophys. Res. Lett.*, *23*(21), 2899–2902, doi:10.1029/96GL02828.
Valdivia, J. A., J. Rogan, V. Muñoz, B. Toledo, and M. Stepanova (2013), The magnetosphere as a complex system, *Adv. Space Res.*, *51*(10), 1934–1941, doi:10.1016/j.asr.2012.04.004.
Vertyagina, Y., and A. Kozlovskiy (2013), Study of solar activity from the position of multifractal analysis, *New Astron.*, *23*, 36–40, doi:10.1016/j.newast.2013.02.006.
Wanliss, J., and V. Uritsky (2010), Understanding bursty behavior in midlatitude geomagnetic activity, *J. Geophys. Res.*, *115*(3), A03215, doi:10.1029/2009JA014642.
Witte, R. S., and J. S. Witte (2009), *Statistics,* chap. 6, 9th ed., Wiley, Hoboken, N. J.
Yang, S., and H. Zhang (2012), Large-scale magnetic helicity fluxes estimated from MDI magnetic synoptic charts over the solar cycle 23, *Astrophys. J.*, *758*(1), 61.
Yurchyshyn, V., H. Wang, and V. Abramenko (2004), Correlation between speeds of coronal mass ejections and the intensity of geomagnetic storms, *Space Weather*, *2*(2), S02001, doi:10.1029/2003SW000020.